Triplet exciton diffusion in metalorganic phosphorescent host-guest systems from first principles

Xander de Vries,[1,*] Pascal Friederich,[2,3,*] Wolfgang Wenzel,[3] Reinder Coehoorn,[1,4] and Peter A. Bobbert[1,4]
[1]*Department of Applied Physics, Eindhoven University of Technology, P.O. Box 513, NL-5600 MB Eindhoven, The Netherlands*
[2]*Department of Chemistry, University of Toronto, 80 St George St, Toronto, Ontario M5S 3H6, Canada*
[3]*Institute of Nanotechnology, Karlsruhe Institute of Technology (KIT), D-76344 Eggenstein-Leopoldshafen, Germany*
[4]*Institute for Complex Molecular Systems, Eindhoven University of Technology, P.O. Box 513, NL-5600 MB Eindhoven, The Netherlands*

(Received 28 February 2019; published 13 May 2019)

We present an *ab initio* computational study of triplet exciton diffusion in four phosphorescent emitters commonly used in organic light-emitting diodes (OLEDs). By kinetic Monte Carlo simulations, triplet diffusion lengths are obtained for these emitters in neat films and as a guest in two different hosts. The triplet transfer rates governing the diffusion contain a transfer integral factor that includes both Förster and Dexter contributions and a Franck-Condon weighted density of vibrational states that includes the coupling to all intramolecular vibrations in a fully quantum mechanical way. We find that at guest concentrations around 10 mol% the Förster transfer contribution is most important. At larger concentrations of about 30–40 mol% the Dexter contribution becomes dominant. We show that obtaining the triplet transfer rates by the semiclassical Marcus theory yields diffusion lengths that are too short and that using a simple cubic lattice in combination with the often used Miller-Abrahams rates instead of using a real morphology with the *ab initio* rates leads to an underestimation of the diffusion lengths due to transfers down in energy that are too slow.

DOI: 10.1103/PhysRevB.99.205201

I. INTRODUCTION

In phosphorescent organic light-emitting diodes (OLEDs), the emission takes place from a host-guest blend in which, often iridium-cored, metalorganic emitter molecules (guests) are incorporated at a small concentration in a host material. In dilute host-guest systems and at low luminance levels, the internal quantum efficiency (IQE) can be close to 100% [1–3]. With increasing guest concentration, the photoluminescence efficiency of host-guest systems is often found to decrease [4], leading to a decrease of the maximum possible IQE of OLEDs. This effect, known as concentration quenching, is attributed to increased triplet exciton diffusion at high guest concentrations, when transfer between the guests is favored due to shorter distances [5,6]. Furthermore, at high luminance levels, triplet exciton diffusion enhances the IQE loss ("roll-off") that occurs due to triplet-triplet annihilation (TTA) and triplet-polaron quenching (TPQ) [7–19].

Triplet exciton diffusion has been extensively studied for purely organic neat-film materials that are commonly used as a host, as an electron or hole transport layer, or a fluorescent emissive layer [20–24]. Due to the long triplet lifetime in such materials and the small intermolecular distances, the diffusion lengths can be of the order of 100 nm. The transfer is commonly viewed as a result of a Dexter-type process [25], with an exponential ($\exp[-2\alpha R]$) distance (R) dependence. Here, α is an effective inverse triplet exciton wave function decay length. In contrast, the diffusion of triplets between iridium-cored phosphorescent emitter molecules, embedded at small concentrations in a host-guest blend, is less well understood. Kawamura *et al.* have suggested that the triplet diffusion leading to concentration quenching is best described as a result of a Förster-type dipole-dipole interaction, with an R^{-6} distance dependence. For molecules containing a heavy-metal atom such as iridium, which due to a strong spin-orbit interaction gives rise to a significant admixture of singlet character in the triplet state, such a mechanism is quantum-mechanically allowed. On the other hand, Ribierre *et al.* conclude that concentration quenching follows an exponential Dexter-type distance dependence [6]. Recently, Ligthart *et al.* have reported that the enhancement of the efficiency loss due to TTA in a phosphorescent host-guest system with varying guest concentration can be understood from both mechanisms [19]. From the latter study, carried out for guest concentrations x_g up to 18 mol%, it follows that triplet exciton diffusion can significantly enhance the efficiency loss due to TTA for x_g larger than approximately 5 mol%.

These experimental studies probe, inevitably, the exciton transfer processes that give rise to triplet diffusion in an ensemble-averaged manner. The development of a mechanistic and predictive model that includes the role of the energetic and positional disorder in the dilute amorphous films and the effect of thermal activation should be based on a theoretical framework for describing, at the molecular scale, the rate of exciton transfer between a donor (D) and an acceptor (A) molecule. From studies of the transfer process by Scholes *et al.* [26–29], the donor-acceptor (D-A) transfer rate k_{DA} is from a Fermi's Golden rule approach [27] given by

$$k_{\mathrm{DA}} = \frac{2\pi}{\hbar} J_{\mathrm{DA}}^2 \rho_{\mathrm{FC}}. \tag{1}$$

Here J_{DA} is the D-A transfer integral, which is dependent on the distance and relative orientation of the donor and acceptor,

*These authors contributed equally to this work.

and ρ_{FC} is the Franck-Condon (FC) weighted density of vibrational states of the D-A pair. The function ρ_{FC} is a sum over all possible combinations of vibronic transitions, at the donor and acceptor molecules, that satisfy the criterion of energetic resonance: $\Delta E \equiv E_{DA^*} - E_{D^*A} = \sum_i n_i \hbar\omega_i$, with ΔE the energy difference between the donor and acceptor triplet states, $\hbar\omega_i$ the vibron energy for mode i, and n_i the number of excited ($n_i < 0$) or absorbed ($n_i > 0$) vibrons for that mode. The asterisk indicates whether the donor or acceptor is excited by the presence of the exciton. Importantly, Eq. (1) shows that the transfer rate can be factorized. The distance dependence of k_{DA} is contained in the factor J_{DA}^2, which contains contributions due to Förster-type and Dexter-type coupling. The temperature and ΔE dependence are contained in ρ_{FC}, which contains the combined contributions of many vibron modes of each molecule. Within simplified approaches, this factor is approximated using a semiclassical approach to the triplet-vibron coupling (Marcus theory [30]), using a quantum-mechanical single-mode approach (Marcus-Levich-Jortner (MLJ) theory [31,32]), or using the Miller-Abrahams (MA) theory [33]. For some classes of materials, the validity of these various approaches has been studied theoretically and experimentally [21,24,34–36]. E.g., Hoffmann *et al.* [36] found that the temperature dependence of triplet diffusion in conjugated polymers is best described by Marcus theory, with a transition to MA theory at lower temperatures. A similar conclusion was drawn by Liu *et al.* for diffusion in the disordered fluorescent small-molecule host-guest system consisting of tris(8-hydroxyquinolinato) aluminum (Alq_3) doped with 4-(dicyanomethylene)-2-methyl-6-julolidyl-9-enyl-4H-pyran (DCM2) [21]. However, for metalorganic phosphorescent emitter molecules, it is presently not clear which of these approaches is most accurate, which type of transfer process (Förster or Dexter) is predominant, and to what extent information about the detailed diffusion mechanism can be gained by studying the guest concentration and temperature dependence of the diffusion-related efficiency loss due to, e.g., concentration quenching or TTA.

Here, we present the results of a first-principles study of the triplet transfer rate k_{DA} between four iridium-cored metalorganic guest molecules that are used frequently as phosphorescent emitters in OLEDs and the resulting diffusion lengths in realistic thin films. The emitter materials studied and their emission colors are

(i) tris[2-phenylpyridinato-C^2,N]iridium(III)($Ir(ppy)_3$, green),

(ii) bis[2-(2-pyridinyl-N)phenyl-C](acetylacetonato)-iridium(III) ($Ir(ppy)_2(acac)$, yellow-green),

(iii) bis(2-benzo[b]thiophen-2-ylpyridine)(acetyl-acetonate)iridium(III) ($Ir(BT)_2(acac)$, yellow),

(iv) bis(2-methyldibenzo[f,h]quinoxaline)(acetylacetonate)iridium(III) ($Ir(MDQ)_2(acac)$, orange-red).

For all these emitter molecules we studied the thermodynamically most stable isomers. For $Ir(ppy)_3$ this is the facial isomer, for the other three emitters we studied the *trans*-N,N isomers. Our study includes the calculation of the triplet transfer integrals J_{DA}, the FC weighted density of vibrational states ρ_{FC}, based on all the vibron energies and on the triplet-vibron coupling for all modes, and the effects of energetic and positional disorder on the diffusion coefficient. The triplet energetic disorder and triplet transfer integrals are calculated for realistic molecular geometries obtained from a Monte Carlo based simulated annealing algorithm. Two commonly used host materials are considered: 4,4'-N,N'-dicarbazole-1,1'-biphenyl (CBP) and tris(4-carbazoyl-9-ylphenyl)amine (TCTA). We show that for guest concentrations above 10 mol%, Dexter transfer is the dominant diffusion mechanism, whereas for concentrations around 10 mol%, the relative contributions of Förster and Dexter transfer depend on the emitter material. Our calculations furthermore show that for these systems Marcus theory predicts triplet transfer rates that are up to one order of magnitude too small.

The structure of the paper is as follows. In Sec. II we present the *ab initio* methods used for calculating the two factors in Eq. (1) and the methods used for obtaining a realistic thin-film morphology with positional and energetic disorder. In Sec. III we present for the four iridium-cored phosphorescent emitters the calculated distance dependence of the triplet transfer rates, interpret these in terms of the commonly used Förster and Dexter models, and compare a full multimode approach with the results of the Marcus, MA, and single-mode MLJ theory. In Sec. IV, we study the consequence of using the calculated transfer rates on the diffusion lengths in the various host-guest systems, incorporating realistic disorder in energy, position, and orientation of the molecules. Section V gives a summary and outlook.

II. THEORETICAL METHODS

In this section we discuss first the theoretical methods that we use to calculate the D-A transfer integrals (subsection A) and the FC weighted densities of vibrational states (subsection B). Using Eq. (1), this provides the transfer rates for each specific D-A pair. Subsequently, we discuss how a realistic host-guest morphology is obtained (subsection C), how the transition dipole moments are calculated (subsection D), and how the guest concentration and temperature dependent diffusion coefficient is obtained (subsection E).

A. Triplet transfer integrals

The triplet exciton transfer integral, J_{DA}, consists of a Coulomb and an exchange contribution [25,27]. The Coulomb contribution can be approximated well by Förster theory [37] when the donor-acceptor distance is sufficiently large with respect to the donor and acceptor molecule size [38]. At guest concentrations used in typical OLEDs ($x_g \leqslant 10$ mol%) this condition is satisfied. The process associated with the exchange contribution is Dexter transfer [25]. In purely organic molecular materials, triplet transfer is governed by the Dexter process because the Coulomb contribution to the transfer integral vanishes due to spin conservation. However, for the iridium-cored metalorganic emitter molecules considered in this work the admixture of singlet character in triplet exciton states is strong enough to facilitate significant Förster transfer. Förster theory describes the Coulomb coupling of excitons as a dipole-dipole interaction [38],

$$J_{DA,\text{Förster}} = \frac{1}{4\pi\epsilon_0\epsilon_r}\frac{\kappa\mu_D\mu_A}{R^3}, \tag{2}$$

with μ_D and μ_A the transition dipole moments of the donor and acceptor molecule, respectively, ϵ_0 the vacuum dielectric permittivity, ϵ_r the relative dielectric constant of the host-guest system, and κ an orientational factor given by

$$\kappa = \vec{\mu}_D \cdot \vec{\mu}_A - 3(\vec{\mu}_D \cdot \vec{R})(\vec{\mu}_A \cdot \vec{R}). \quad (3)$$

Within first order perturbation theory, the Dexter transfer integral $J_{DA,Dexter}$ is equal to the direct exchange integral $J_{DA,exchange,d}$, between the excited donor (D^*A) and the excited acceptor (DA^*) states. In order to obtain this contribution, the coupling matrix elements of emitter molecule dimers were calculated using the Löwdin orthogonalization based on single-molecule Kohn-Sham molecular orbitals and the Fock and overlap matrix from the molecular dimer [39,40].

Previous studies have shown that contributions of intermediate charge transfer (CT) states of the type D^+A^- or D^-A^+ can strongly enhance the transfer integral for Dexter coupling [27,41]. We add the contribution of intermediate CT states to the total transfer integral for Dexter coupling as described in Ref. [41]:

$$J_{DA,Dexter} = J_{DA,exchange,d} + \frac{1}{2}\sum_{CT\ states} J_{D,CT}J_{CT,A} \times \left[\frac{1}{E_{CT} - E_T^D} - \frac{1}{E_{CT} - E_T^A}\right], \quad (4)$$

where the coupling integrals to the CT states are given by $J_{D,CT}$ and $J_{CT,A}$, and the energies of the donor and acceptor triplet and CT states by E_T^D, E_T^A, and E_{CT}, respectively. We show in Sec. III that for the iridium-cored emitters studied in this work the CT-state contributions enhance the Dexter transfer integrals significantly.

B. Vibronic coupling

The FC weighted density of vibrational states ρ_{FC} in Eq. (1) sums over all possible combinations of vibrational modes of both molecules that enable the triplet transfer. The triplet-vibron coupling is often described using Marcus theory, within which the coupling to vibrational modes is treated semiclassically. The transfer rate is then given by $k_{DA,Marcus} = (2\pi/\hbar)J_{DA}^2\rho_{Marcus}$, with

$$\rho_{Marcus} = \frac{1}{\sqrt{4\pi\lambda k_B T}} \exp\left(-\frac{(\Delta E + \lambda)^2}{4\lambda k_B T}\right), \quad (5)$$

where k_B is the Boltzmann constant, T the temperature, and λ the reorganization energy. Within a harmonic approximation, the reorganization energy is equal to a sum over all the vibron mode energies, weighted by their dimensionless coupling strength S_i, the Huang-Rhys parameter:

$$\lambda = 2\sum_i S_i \hbar\omega_i. \quad (6)$$

The factor 2 accounts for the modes of the donor and acceptor molecules, under the assumption that the mode energies and couplings are the same for both molecules. It has been recognized by Siders and Marcus [42] that the Marcus theory does not yield correct results for the case of strong coupling ($S_i > 1$) to modes with relatively high energy, i.e., when $\hbar\omega_i > 0.05$ eV, well above $k_B T$ at room temperature.

Exciton transfer for coupling to a single high-energy mode is described within the Marcus-Levich-Jortner (MLJ) theory [31,32]. Historically, a restriction to a single-mode formulation has often been made in view of the intractable number of degrees of freedom in ρ_{FC} when including combinations of all vibron modes in the molecules. Another limiting factor is the calculation of the vibron modes and vibron couplings for medium-sized molecules (~100 atoms). Using modern computational methods and resources both issues can be tackled. Vibron energies and couplings can be calculated for large molecules using density functional theory (DFT). Calculating ρ_{FC} can be done by using Monte Carlo sampling techniques [43] or by transforming the problem to the time domain and numerically calculating the resulting time integral [44,45]. Here, ρ_{FC} is calculated using a method developed in our previous work on charge transfer [45]. In this method all vibron energies ($\hbar\omega_i$) and couplings (S_i) are calculated with DFT and ρ_{FC} is transformed into an integral in the time domain that is solved numerically. The integral involves a broadening parameter (λ_{cl}), which can be physically interpreted as a very small reorganization contribution that is treated classically. This slightly broadens the vibronic levels and makes the triplet transfer energetically allowed. In our previous work we showed that for small values the transfer rate is independent of λ_{cl}. The full expression of ρ_{FC} is given in Appendix A of Ref. [45]. A comparison with the MLJ theory is given in Appendix B of the same paper.

In Fig. 2, we show ρ_{FC} for the case of coupling between identical donor and acceptor molecules, each with one quantum-mechanically treated vibron mode with an energy $\hbar\omega$ and for a combined (donor-acceptor) coupling parameter $S_{DA} = 2S$. In panels (a) and (c), the vibron energy is equal to the thermal energy ($\hbar\omega = k_B T$). In that case, and more generally for $\hbar\omega \lesssim k_B T$, Marcus theory provides a good approximation. In panels (b) and (d), the vibron energy is significantly (4×) larger than the thermal energy so that Marcus theory no longer applies. Panel (d) corresponds to a modest vibronic coupling strength ($S_{DA} = 1$), which is common for charges [45]. Panel (b) corresponds to a strong vibronic coupling strength ($S_{DA} = 4$), which in Sec. III will be shown to be realistically applicable to triplets on the metalorganic emitter molecules studied in this work. The diffusion in a disordered organic material consists of a sequence of transfers between molecules with random energies, often distributed according to a Gaussian density of states. As the width (standard deviation σ_T) of the density of states is only approximately 0.05 eV, a typical triplet transfer process is expected to occur within the energy range -0.05 eV $< \Delta E < +0.05$ eV. Panel (d) shows that at a modest vibronic coupling strength ($S_{DA} = 1$), the approximate and exact densities of states ρ_{Marcus} and ρ_{FC}, respectively, have very similar values around $\Delta E = 0$. This was found to explain why charge mobilities calculated using Marcus theory do not differ much from those calculated with a fully quantum-mechanical approach [45]. However, panel (b) shows that for a strong coupling strength, the quantum-mechanically exact rate is significantly larger than the Marcus rate. The enhancement is due to nuclear tunneling [46].

The triplet-vibron couplings of the four emitter molecules in Fig. 1 were calculated using open-shell DFT employing the B3LYP functional [47] and a def2-SVP basis set [48],

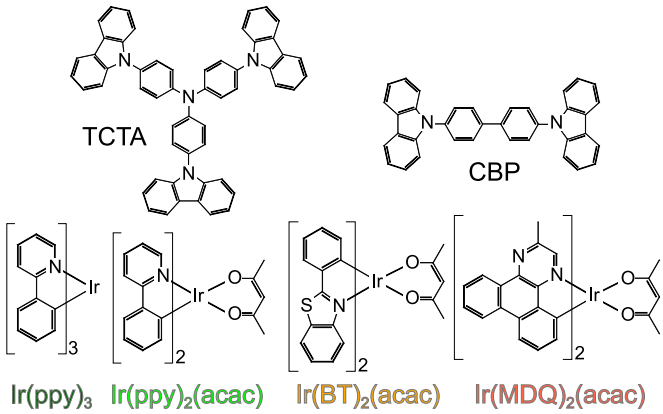

FIG. 1. Chemical structures of the two host materials (CBP and TCTA) and four emitter materials [$Ir(ppy)_3$, $Ir(ppy)_2(acac)$, $Ir(BT)_2(acac)$, $Ir(MDQ)_2(acac)$] studied in this work.

using corresponding effective core potentials as employed in the ORCA [49] package. The B3LYP functional was chosen because it has been successfully used in calculating the lifetimes and triplet energies of iridium cored emitters [50,51] and also performs rather well in the calculation of reorganization energies for electrons and holes [52]. The dimensionless triplet-vibron couplings (S_i) and vibron mode energies ($\hbar\omega_i$) were obtained from calculations of the Hessians and gradients in the triplet and ground state geometries, as detailed in Ref. [45] for the case of charges.

C. Calculation of the morphology and energetic disorder

To generate microscopic morphologies, a Metropolis Monte Carlo based simulated annealing algorithm [53] was used to generate atomistically resolved amorphous samples of the two host and four emitter materials. We generated pure guest and mixed host-guest morphologies with a guest concentration of 10 mol%. The details of the method can be found in the Supplemental Material (SM) [54].

To obtain distributions of triplet energies of host and guest molecules, we performed DFT-based calculations using the Quantum Patch method [55]. These calculations were performed with open-shell DFT using the Turbomole package [56] with the B3LYP functional [47] and def2-SVP basis set [48]. Due to the effect of the environment the energetic disorder is slightly different for the CBP, TCTA, and neat film systems. In the CBP films with 10 mol% emitter, the energetic disorder is 0.058, 0.044, 0.037, and 0.052 eV for $Ir(ppy)_3$, $Ir(ppy)_2(acac)$, $Ir(BT)_2(acac)$, and $Ir(MDQ)_2(acac)$, respectively. In the 100 mol% emitter films, the energetic disorder is 0.050, 0.056, 0.032, and 0.066 eV, respectively. Details about the calculation method and triplet energies and energetic disorder values for TCTA can be found in the SM [54].

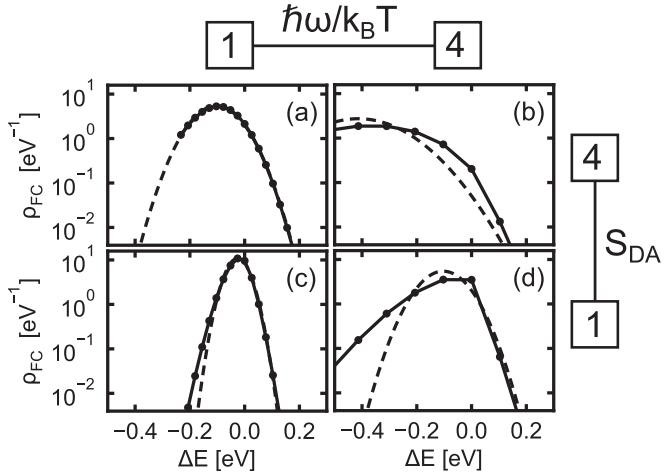

FIG. 2. Dependence of the FC weighted density of vibrational states, to which the triplet exciton transfer rate is proportional [see Eq. (1)], on the energy difference ΔE between the final and initial state, for the case of coupling to a single quantum-mechanical mode with energy $\hbar\omega$ and with a coupling strength S ($S_{DA} = 2S$). Panels (a)–(d) give the results for four combinations of these parameters. The points are prefactors at integer multiples of $\hbar\omega$ for ΔE of delta functions in ρ_{FC} divided by $\hbar\omega$. The full lines connect these points. The dashed curves give the classical Marcus result, obtained from Eqs. (5) and (6).

D. Transition dipole moments and lifetimes

The transition dipole moments for the different emitter molecules are required in order to calculate the Förster transfer integrals as given in Eq. (2) and to determine the radiative lifetimes of the triplet excitons. We start with calculating the triplet energy E_T as the difference between the spin-restricted and geometrically relaxed DFT triplet state energy and the ground state DFT energy, both calculated in the zeroth order relativistic approximation (ZORA) with scalar relativistic corrections; see Table I). These energies are quite close to the experimental values [19]. Next, we calculate with time-dependent DFT (TD-DFT), including spin-orbit coupling in the ZORA approximation [57], the energy splitting of the three triplet states and their transition dipole moments in the geometry of the spin-restricted DFT calculations. In the calculations, the segmented all-electron relativistically controlled (SARC) basis set for the ZORA method was used for the iridium atom [58]. For the other atoms the 6-31G basis set was used. In order to describe the effect of the environment, a conductorlike polarizable continuum model (CPCM) [59] was used with $\epsilon_r = 3$, close to the relative dielectric constant measured in CBP and TCTA [60,61], and $n = \sqrt{\epsilon_r}$. All methods and basis sets are implemented in the ORCA [49] package that was used for the calculations.

Using the calculated transition dipole moments μ_i (i = I, II, III), the radiative lifetime τ of the triplet states can be calculated by [50,62,63]

$$\frac{1}{\tau_i} = \frac{4}{3}\frac{\mu_i^2 n^2}{4\pi\epsilon_0\hbar}\left(\frac{E_T}{\hbar c}\right)^3, \tag{7}$$

where, because of their small energy splittings, we can take in this expression the energies of all three triplet states equal to E_T. The lifetimes of the three triplet states are reported in Table I. We assume that transitions between the three triplet states induced by vibrations occur sufficiently rapidly to establish thermal equilibrium in the occupations of the three triplet levels before decay of the exciton or transfer to another molecule. The Boltzmann-averaged effective radiative

TABLE I. Calculated triplet energies, triplet level splittings, triplet lifetimes [Eq. (7)], Boltzmann-averaged lifetimes [Eq. (8)], and effective transition dipole moments [Eq. (9)] for the different emitter molecules. The values in parentheses are obtained from experiments on the emitters in a TCTA film [19] (the results in a CBP film are almost the same).

	E_T (eV)	$\Delta E_{II\text{-}I}$ (meV)	$\Delta E_{III\text{-}I}$ (meV)	τ_I (μs)	τ_{II} (μs)	τ_{III} (μs)	τ (μs)	μ (D)
$Ir(ppy)_3$	2.51 (2.43)	14.6	40.6	94.8	10.4	0.15	1.26 (1.22)	0.540
$Ir(ppy)_2(acac)$	2.43 (2.38)	6.67	25.0	7.15	18.0	0.35	1.73 (1.38)	0.411
$Ir(BT)_2(acac)$	2.16 (2.23)	3.55	34.4	60.1	284	0.29	2.39 (1.31)	0.490
$Ir(MDQ)_2(acac)$	2.05 (2.05)	8.79	17.5	13.1	9.62	0.50	1.93 (1.65)	0.474

lifetime then becomes

$$\tau^{-1} = \frac{\tau_I^{-1} + \tau_{II}^{-1} \exp\left(\frac{-\Delta E_{II\text{-}I}}{k_B T}\right) + \tau_{III}^{-1} \exp\left(\frac{-\Delta E_{III\text{-}I}}{k_B T}\right)}{1 + \exp\left(\frac{-\Delta E_{II\text{-}I}}{k_B T}\right) + \exp\left(\frac{-\Delta E_{III\text{-}I}}{k_B T}\right)}. \quad (8)$$

The average triplet lifetimes of the different emitter molecules at 300 K are given in Table I, together with experimental values [19]. The calculated and experimental values are quite close. The shorter experimental lifetimes for $Ir(BT)_2(acac)$ and $Ir(MDQ)_2(acac)$ can be attributed to significant nonradiative decay rates in these molecules: The photoluminescence (PL) efficiencies of $Ir(BT)_2(acac)$ and $Ir(MDQ)_2(acac)$ are 0.65 [64] and 0.77 [65], respectively, whereas the PL efficiencies of $Ir(ppy)_3$ and $Ir(ppy)_2(acac)$ are close to 1 [2,64].

In order to calculate the Förster transfer integrals we should use Eq. (2). Because the three triplet levels of the emitter molecules can all be thermally occupied (see above) we need, in principle, to average the Förster transfer integrals over all possible transitions from the three levels of the donor to the three levels of the acceptor molecule. Taking into account all the transitions between the triplet levels would involve an average over nine different Förster transfer integrals. However, we can readily see from Table I that most of these contributions will be small, since for each molecule the lifetime of the highest triplet state (T_{III}) is at least 20 times smaller than the other lifetimes. Since the lifetime is proportional to the square of the transition dipole moment, the strongest Förster transfer integral contribution is at least 20 times larger than the other contributions. To avoid having to sum over all transitions, and having to take all the correlations in orientations of the molecules into account, we therefore only take the donor T_{III} to acceptor T_{III} Förster transfer integral into account. This assumption leads to an error in the transfer rate of at most 15% [for $Ir(MDQ)_2(acac)$], which is on the order of the diffusion length error bars (see Sec. IV). The Förster contribution to the triplet transfer rate should then be Boltzmann weighted by the occupation of the highest triplet level. Since the rate is proportional to the fourth power of the transition dipole (assuming that $\mu_D = \mu_A$) we take as effective transition dipole moment

$$\mu = \left(\frac{\exp\left(\frac{-\Delta E_{III\text{-}I}}{k_B T}\right)}{1 + \exp\left(\frac{-\Delta E_{II\text{-}I}}{k_B T}\right) + \exp\left(\frac{-\Delta E_{III\text{-}I}}{k_B T}\right)}\right)^{\frac{1}{4}} \mu_{III}. \quad (9)$$

These transition dipole are given in the last column of Table I.

E. Calculation of the diffusion length

Calculations of the guest concentration dependence of the triplet exciton diffusion length, L_D, are carried out for each of the eight host-guest systems and four pure guest systems studied. For that purpose, we perform random walker kinetic Monte Carlo (KMC) simulations in a simulation box of $50 \times 50 \times 50$ nm^3 with periodic boundary conditions, with a morphology obtained using the morphology expansion method discussed in the SM [54]. Each emitter molecule in the box is assigned a triplet energy drawn from a Gaussian density of states with a standard deviation σ_T (see subsection C), a randomly chosen orientation, and the transition dipole moment given in Table I. For each emitter pair, the transfer rate is obtained using Eq. (1), with the squared transfer integrals $[J_{DA}^2 = (J_{Dexter} + J_{Förster})^2]$ and the FC weighted density of vibrational states ρ_{FC} calculated from the energies, distances, orientations, and transition dipole moments of the molecules in the box. After that, the random walk of a triplet exciton, introduced at a randomly chosen position, is followed throughout the simulation, until the exciton decays. After each decay a new triplet exciton is introduced, until a sufficient level of statistical accuracy is obtained.

From diffusion theory, the probability (P) distribution of diffusion distances in the positive or negative x directions is for ordered systems given by

$$P(|x|) = \frac{1}{2L_{D,1D}} \exp\left[-\frac{|x|}{L_{D,1D}}\right], \quad (10)$$

with L_D the one-dimensional diffusion length. For disordered molecular systems that contain a certain fraction of strongly isolated sites from which no diffusion takes place, such as the host-guest systems studied in this work, it is not correct anymore to obtain the diffusion length from the root-mean-square displacement [66]. However, $P(|x|)$ is still proportional to $\exp(-|x|/L_D)$. We therefore define L_D as the average of the values obtained from the exponential decrease of the emission profiles in the positive and negative x, y, and z directions. In order to obtain the three-dimensional diffusion length, we multiply the one-dimensional diffusion length by a factor $\sqrt{3}$, so that the diffusion lengths reported are obtained from Eq. (10) and $L_D = \sqrt{3} L_{D,1D}$.

III. RESULTS

A. Transfer integrals

Figures 3(a) and 3(b) show for neat (100 mol% emitter) films of $Ir(ppy)_3$, $Ir(ppy)_2(acac)$, $Ir(BT)_2(acac)$, and

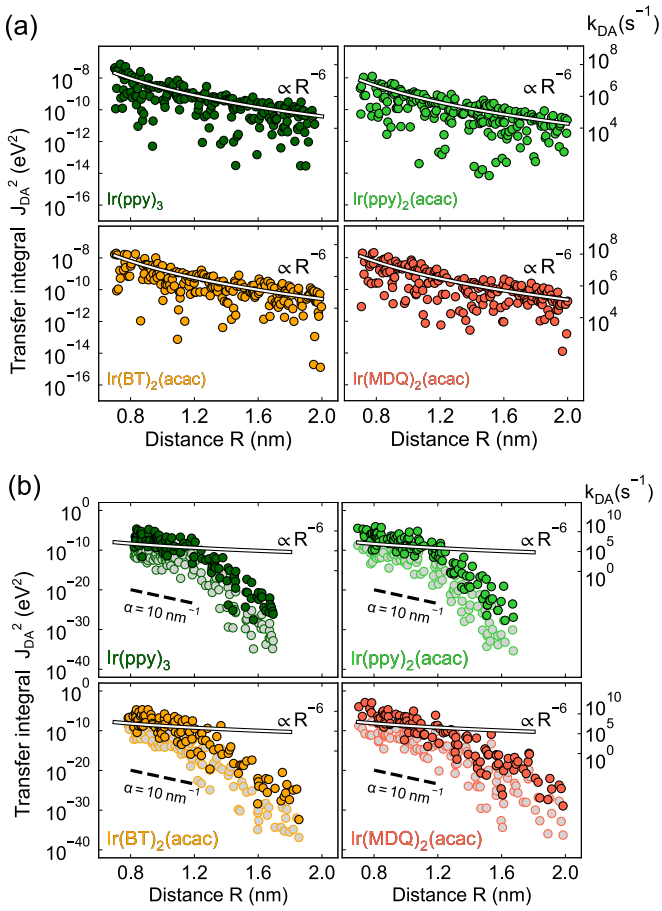

FIG. 3. (a) Squared Förster transfer integrals for triplet excitons as a function of the center-of-mass distance between two emitter molecules, calculated for 100 mol% films of the four emitter materials studied in this work. The Förster transfer integrals were obtained by generating random orientations of the molecules. The white solid line shows the result for a squared orientational factor $\kappa^2 = \langle\kappa^2\rangle = 2/3$. The y-axis to the right shows the rate k_{DA} for a transfer with equal D and A triplet energies. (b) Squared Dexter transfer integrals for triplet excitons. The shaded circles show the result when neglecting the CT-state contribution in Eq. (4). The dashed line indicates the transfer integral decrease expected in the case of an exponential $\exp(-2\alpha R)$ distance dependence, with $\alpha = 10$ nm^{-1}. The y-axis to the right shows the rate k_{DA} for a transfer with equal D and A triplet energies. The white solid line shows the same result as in (a).

Ir(MDQ)$_2$(acac) the calculated center-of-mass distance (R) dependence of the absolute values of the squared transfer integrals, for Förster-type and Dexter-type coupling, respectively. The full white curves in Fig. 3(a) indicate the R^{-6} distance dependence of the decay expected for Förster-type transfer. The dashed lines in Fig. 3(b) indicate the exponential ($\exp[-2\alpha R]$) decay expected for Dexter-type transfer, for $\alpha = 10$ nm^{-1}. Figure 3(b) shows that for intermolecular distances larger than 1.5 nm the transfer integrals for Förster transfer are for all emitters much larger than those for Dexter transfer. The molecular density of the films is around 1.4 nm^{-3}. In neat films, the average nearest-neighbor distance is therefore below 1 nm, so that Dexter transfer is then the dominant diffusion mechanism. This will be confirmed in Sec. IV.

Transfer integrals have also been calculated for 10 mol% films with a CBP and TCTA host (see SM [54]). The transfer integrals are comparable to those of the 100% systems, although the statistics is less good. At a 10% guest concentration, the average emitter-emitter separation is approximately 2 nm. One could therefore expect that Förster transfer is then the dominant diffusion mechanism. However, we will show in Sec. IV that as a result of the randomness of the spatial distribution of emitter sites, leading locally to much shorter distances between the emitters, the Dexter transfer contribution is then still significant.

Figure 3(b) also shows the significance of the CT-state contributions described in Eq. (4). Including the CT-state coupling enhances the Dexter transfer integrals by at least two orders of magnitude. The resulting effect on the diffusion length will be discussed in Sec. IV. For Ir(MDQ)$_2$(acac), the Dexter coupling extends over a larger distance than for the other emitters considered. The difference can be attributed to the larger molecular size of this emitter.

B. Vibronic coupling and energy dependence of the transfer rate

Figure 4(a) shows for the emitter molecules studied in this work the cumulative triplet-vibron coupling strength. Each step in the figure, at a vibron energy $\hbar\omega_i$, gives the contribution $\lambda_i = S_i\hbar\omega_i$ of mode i to the total reorganization energy per molecule. The figure shows that the four emitters can be separated into two groups. For Ir(ppy)$_2$(acac) and Ir(MDQ)$_2$(acac), vibron modes with energies around 25 meV already contribute to about half of the total reorganization energy per molecule. In contrast, for Ir(BT)$_2$(acac) and Ir(ppy)$_3$, the high-energy vibrons that are due to C-C bond stretching, from 125 meV to 200 meV, contribute most. Furthermore, the total reorganization energy is significantly larger for Ir(BT)$_2$(acac) and Ir(ppy)$_3$ than for Ir(ppy)$_2$(acac) and Ir(MDQ)$_2$(acac).

The contribution of low-energy modes, below 0.025 eV, is for all four emitters found to be very small. In contrast, modes with such low energies were found to contribute strongly to the electron-vibron and hole-vibron coupling for the purely organic materials NPB, TCTA, and spiro-DPVBi [45].

Figure 4(b) (full curves) shows for each of the materials studied in this work the energy (ΔE) dependence of the triplet transfer rate for the case of Förster transfer at 300 K between two molecules at a distance of 1 nm, averaged over all combinations of relative molecular orientations [i.e., based on the transfer integral given by the white solid curve in Fig. 3(a)]. We note that the transfer integral is not dependent on the energy difference between D and A, so that the ΔE dependence is equal for Förster and Dexter transfer. The short-dashed curves give, for comparison, the rates obtained from Marcus theory using the total reorganization energy for the transfer process, $\lambda = 2\sum_i \lambda_i$. The differences between the two groups of emitters, mentioned earlier, are evident. While the triplet transfer rate for Ir(ppy)$_2$(acac) and Ir(MDQ)$_2$(acac) is reasonably approximated by the Marcus rate (the deviation at $\Delta E = 0$ is approximately a factor of two), the Marcus theory underestimates for Ir(BT)$_2$(acac) and

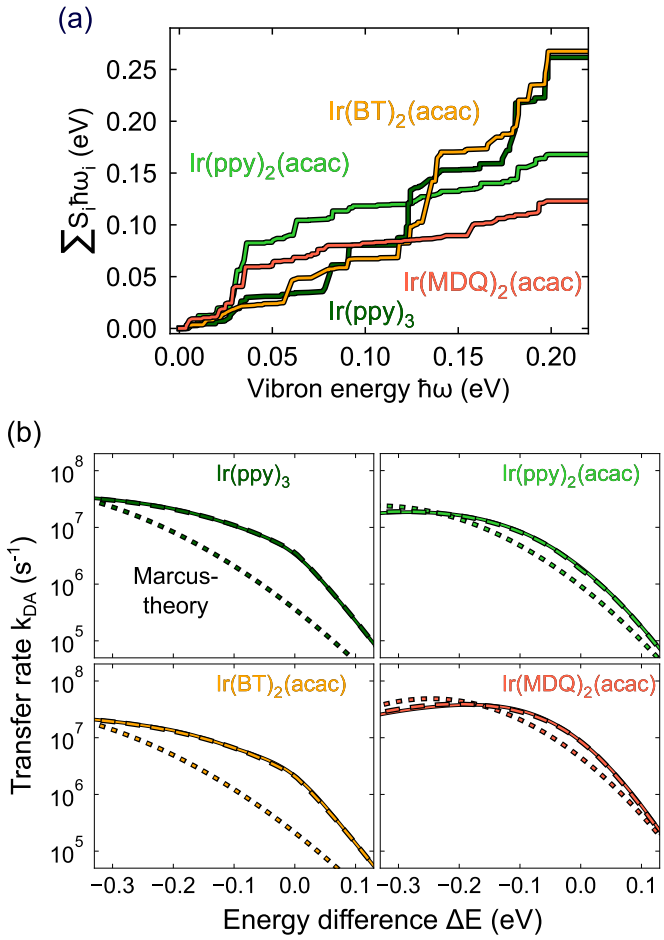

FIG. 4. (a) Cumulative vibronic coupling energy per molecule as a function of the vibron energy for Ir(ppy)$_2$(acac) (light green), Ir(BT)$_2$(acac) (orange), Ir(ppy)$_3$ (dark green), and Ir(MDQ)$_2$(acac) (red). (b) Quantum-mechanical multimode rate (full curve), single-mode approximation [Eq. (11), dashed curve], and Marcus rate [Eq. (5), dotted curve] of triplet transfer for the four investigated emitters at 300 K. The Förster coupling given by Eq. (2) was used for two molecules at 1 nm center-of-mass distance, with $\epsilon_r = 3$, $\mu_D = \mu_A = \mu$ from Table I, and $\kappa^2 = 2/3$.

Ir(ppy)$_3$ the rate by about one order of magnitude. At lower temperatures, the underestimation by the Marcus theory is for all iridium emitters even more pronounced. At 150 K, the underestimation by the Marcus rate is one order of magnitude for Ir(ppy)$_2$(acac) and Ir(MDQ)$_2$(acac) and almost three orders of magnitude for Ir(BT)$_2$(acac) and Ir(ppy)$_3$ (see the SM [54]). This shows that nuclear tunneling, which for charges is often only at low temperatures of importance [45], is for triplet excitons already significant at room temperatures, in particular when strongly coupled high-energy modes are involved, such as for Ir(BT)$_2$(acac) and Ir(ppy)$_3$. Treating these modes classically, instead of quantum mechanically, leads to a strong underestimation of the transfer rate.

Figure 4(b) also shows that for all systems studied the transfer rate is a smooth function of the energy difference ΔE between the final and initial states. This is due to the multimode nature of the triplet transfer process, as would already be expected from Fig. 4(a). We note that for electron or hole hopping in purely organic systems, the rate was in some cases found to be determined predominantly by a single vibron mode, leading to an oscillatory component in the dependence on ΔE [45].

The ΔE dependence of the transfer rate is quite insensitive to the detailed contributions of individual modes. Actually, it is possible to describe the transfer as a result of coupling with a single (effective) high-energy mode, combined with coupling to a continuum of lower-energy modes. Application of the single-mode MLJ theory, with a Boltzmann factor added for $\Delta E > 0$ in order to satisfy detailed balance, then leads to an effective FC weighted vibrational density of states

$$\rho_{\mathrm{FC,eff}}(\Delta E) = \frac{1}{\hbar\omega_{\mathrm{eff}}} \frac{\exp(-S_{\mathrm{eff}})}{\Gamma(\Delta E/\hbar\omega_{\mathrm{eff}} + 1)} \exp\left(\frac{\Delta E \ \ln(S_{\mathrm{eff}})}{\hbar\omega_{\mathrm{eff}}}\right) \times \exp\left(-\frac{\Delta E + |\Delta E|}{2k_B T}\right), \tag{11}$$

corresponding to a vibronic coupling with a strength S_{eff} to a single mode with an energy $\hbar\omega_{\mathrm{eff}}$. The two effective parameters, S_{eff} and $\hbar\omega_{\mathrm{eff}}$, are obtained from a fit of $\rho_{\mathrm{FC,eff}}(\Delta E)$ to the *ab initio* function $\rho_{\mathrm{FC}}(\Delta E)$, under the constraint that $S_{\mathrm{eff}}\hbar\omega_{\mathrm{eff}} = \lambda$, with $\lambda = 2\sum_i S_i\hbar\omega_i$ the total reorganization energy. For the studied emitters, these parameters are given in Table II. We note that S_{eff} contains the contributions from *both* molecules and that the value $S_{\mathrm{eff}}/2$ per molecule is not simply equal to the ratio of the first and second vibronic emission peaks because of the multimode nature of the triplet-vibron coupling. This means that the effective parameters introduced in Eq. (11) cannot straightforwardly be obtained from emission spectra of the emitter molecules.

Figure 4(b) (long-dashed curves) shows that this approximation agrees well with the *ab initio* result. A first benefit of deriving the effective parameters $\hbar\omega_{\mathrm{eff}}$ and S_{eff} is that from their value the location of the transfer process in the diagram shown in Fig. 1 may be quantified. Secondly, the approximation provides a convenient method for describing the rate using a compact expression that may be readily used in, e.g., KMC device simulations. We note that the effective parameters are temperature dependent, as may be seen from Table II. At lower temperature, the quantized nature of ever lower energy modes must be included, so that $\hbar\omega_{\mathrm{eff}}$ becomes smaller. S_{eff} becomes then larger, as the product $S_{\mathrm{eff}}\hbar\omega_{\mathrm{eff}}$ remains equal to the (temperature independent) reorganization energy λ. The overall effect is a predicted decrease of the transfer rate with decreasing temperature, as may be seen from the one but last column in Table II for the case of transfer with $\Delta E = 0$. However, the temperature dependence is much weaker than that following from Marcus theory [Eq. (5)].

Similar to our finding that for commonly used iridium-cored metalorganic phosphorescent emitters the triplet-vibron coupling is strong ($S_{\mathrm{eff}} \gg 1$), theoretical work by Pabst *et al.* has revealed that also for purely organic materials used in organic electronic devices the triplet reorganization energies are high (0.6–0.8 eV per D-A pair) and at least twice as large as those for electrons and holes (0.2–0.4 eV per D-A pair) [67,68]. The authors found that the triplet wave functions are considerably more localized on the molecules than the single electron or hole wave functions. Highly localized triplet wave functions lead to strong C-C bond distortions, resulting in a

TABLE II. Total reorganization energy λ for D-A transfer between the investigated emitters, and effective vibron energy $\hbar\omega_{\text{eff}}$ and triplet-vibron coupling strength S_{eff} at 300 K|150 K that provide with $\rho_{\text{FC,eff}}$ from Eq. (11) a best fit to the *ab initio* FC weighted vibrational density of states ρ_{FC} that enters Eq. (1). The one but last column gives $\rho_{\text{FC,eff}}$ for $\Delta E = 0$. The last column gives the Förster radius $R_{\text{F},0}$ for transfer with $\Delta E = 0$ from Eq. (13) at 300 K.

	λ (eV)	$\hbar\omega_{\text{eff}}$ (eV)	S_{eff}	$\rho_{\text{FC,eff},0}$ (eV^{-1})	$R_{\text{F},0}$ (nm)
Ir(ppy)_3	0.524	0.135|0.123	3.88|4.26	0.153|0.115	1.29
$\text{Ir(ppy)}_2\text{(acac)}$	0.336	0.085|0.061	3.95|5.51	0.226|0.066	1.22
$\text{Ir(BT)}_2\text{(acac)}$	0.535	0.133|0.127	4.02|4.22	0.134|0.116	1.31
$\text{Ir(MDQ)}_2\text{(acac)}$	0.246	0.083|0.063	2.96|3.91	0.624|0.318	1.60

strong coupling with the corresponding high-energy vibrons. We find a similar trend in the case of the phosphorescent iridium molecules studied in this work. For Ir(ppy)_3 and $\text{Ir(BT)}_2\text{(acac)}$, the triplet wave function extends over the iridium core and one of the ligands, while for $\text{Ir(ppy)}_2\text{(acac)}$ and $\text{Ir(MDQ)}_2\text{(acac)}$, the triplet wave function extends over the iridium core and both of the ppy or MDQ ligands. The different degrees of delocalization are reflected in the triplet reorganization energy, which is lower for $\text{Ir(ppy)}_2\text{(acac)}$ and $\text{Ir(MDQ)}_2\text{(acac)}$, with smaller contributions from the C-C vibrons; see Fig. 4(a). Plots of the triplet wave functions are given in the SM [54].

C. Förster radius

In analyses of experiments probing Förster transfer, the effective (ensemble-averaged) rate is conventionally expressed as

$$k_{\text{Förster}}(R) = \frac{1}{\tau}\left(\frac{R_{\text{F}}}{R}\right)^6, \tag{12}$$

with τ the lifetime of the exciton at the donor and R_{F} the so-called Förster radius. At the microscopic level, the distribution of D-A transfer integrals and D-A triplet energy differences leads to a distribution of pair-specific Förster radii. The Förster radius for transfer between molecules for which $\Delta E = 0$ may from Eqs. (1), (2), (11), and (12) be written as

$$R_{\text{F},0}(\kappa) \cong \left(\frac{\kappa^2\mu^4\tau}{8\pi\epsilon_0^2\epsilon_{\text{r}}^2\hbar}\frac{\exp(-S_{\text{eff}})}{\hbar\omega_{\text{eff}}}\right)^{1/6}. \tag{13}$$

The Förster radii $R_{\text{F},0}$ calculated with Eq. (13) are reported in Table II. These Förster radii are calculated at room temperature for $\kappa^2 = \langle\kappa^2\rangle = 2/3$ (the isotropic orientation value [38]). The values for μ and E_{T} are obtained from Table I, and the values of $\hbar\omega_{\text{eff}}$ and S_{eff} from Table II. For Ir(ppy)_3, the value of $R_{\text{F},0} = 1.29$ nm is slightly smaller than the Förster radii of 1.4 nm and 1.8 nm that were deduced by Kawamura *et al.* [4] from concentration quenching and spectral overlap measurements, respectively. For $\text{Ir(Btp)}_2\text{(acac)}$, the same experimental studies yielded Förster radii of 0.8 nm for a concentration quenching study, and 1.5 nm for a spectral overlap measurement, whereas we find a value of $R_{\text{F},0} = 1.31$ nm for the similar molecule $\text{Ir(BT)}_2\text{(acac)}$. The calculated values of the Förster radius for $\Delta E = 0$ do not include the effects of energetic relaxation in the triplet density of states. These effects can be important because in diffusion experiments and spectral overlap measurements relaxation plays a role. The role of relaxation in diffusion will be studied in the next section.

D. Dexter rate

The Dexter transfer rate is often expressed as

$$k_{\text{Dexter}}(R) = k_0\exp(-2\alpha R), \tag{14}$$

where α is the wave function attenuation parameter and R is the D-A distance. The prefactor k_0 includes the vibronic factor ρ_{FC} discussed previously and a transfer integral contribution that is extrapolated to $R = 0$. In Eq. (14), the orientations of the donor and acceptor molecules are not taken into account. Previous results have shown that the triplet transfer integral is highly dependent on orientation [41]. This is confirmed by our calculations. At a fixed distance, the squared transfer integrals shown in Fig. 3(b) show a value spread of many orders of magnitude. Between 0.8 to 1.5 nm the disorder in the squared transfer integrals is much stronger than the distance dependence. Above 1.5 nm the coupling decreases rapidly, which implies that Dexter transfer with $R > 1.5$ nm practically does not occur. For the case of Dexter transfer we therefore expect diffusion over significant distances only for average guest-guest distances smaller than 1.5 nm. In the next section we will look at the emitter concentration dependence of the diffusion process and show that this is indeed the case.

IV. DIFFUSION LENGTH—CONCENTRATION AND TEMPERATURE DEPENDENCE

A. KMC simulations for a realistic morphology

Figure 5(a) shows the results of calculations of the triplet diffusion lengths for CBP films with 10 mol% of Ir(ppy)_3, $\text{Ir(ppy)}_2\text{(acac)}$, $\text{Ir(BT)}_2\text{(acac)}$, and $\text{Ir(MDQ)}_2\text{(acac)}$, obtained using KMC simulations for a realistic morphology. The diffusion lengths taking into account Dexter and Förster transfer ("full") vary from 1.5–2.5 nm. Consistent with these small values, which are on the order of the nearest-neighbor to next-nearest-neighbor distance, we find that many triplets introduced in the system do not diffuse but decay radiatively on the molecule at which they have been generated. The figure also gives the results when including only Dexter transfer ($J_{\text{DA}} = J_{\text{Dexter}}$) and only Förster transfer ($J_{\text{DA}} = J_{\text{Förster}}$). In all cases the Dexter-only values are about a factor of two smaller than the Förster-only contributions. This can be explained by the fact that at 10 mol% the average guest-guest distance is on the order of 2 nm. As can be seen from Fig. 3, the

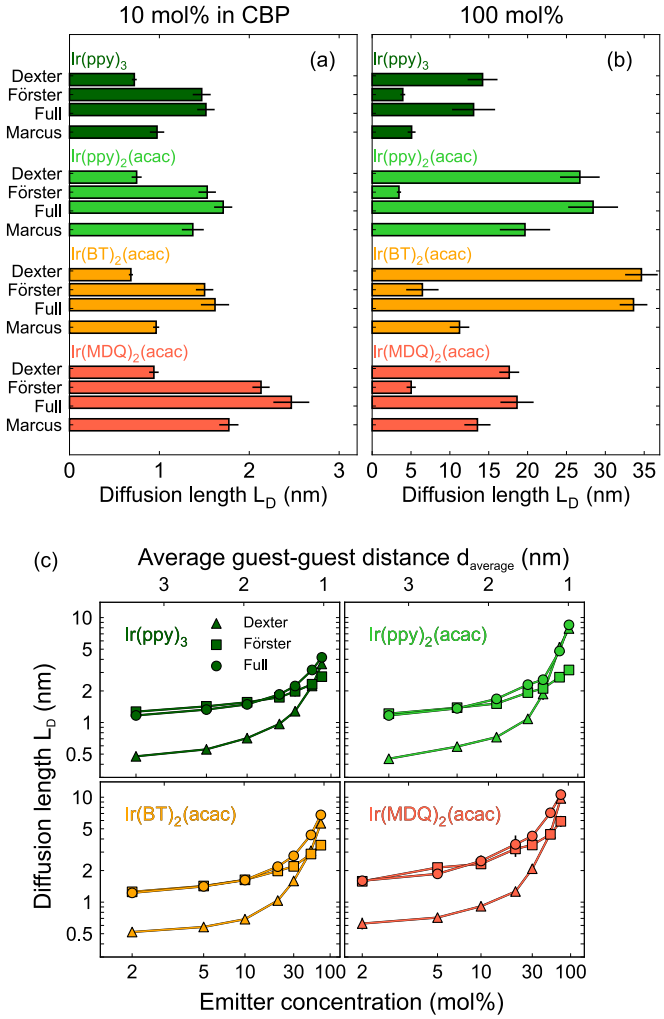

FIG. 5. Triplet diffusion lengths at room temperature for (a) 10 mol% and (b) 100 mol% films of the four emitter materials studied in this work, obtained from KMC simulations for a realistic morphology. A comparison is made between results obtained using Dexter-only ($J_{DA} = J_{Dexter}$), Förster-only ($J_{DA} = J_{Förster}$), and full ($J_{DA} = J_{Dexter} + J_{Förster}$) transfer integrals. The Marcus result shows the effect of taking $J_{DA} = J_{Dexter} + J_{Förster}$ and using the semiclassical Marcus expression ρ_{Marcus} [Eq. (5)] instead of ρ_{FC}. The FC weighted density of vibrational states (ρ_{FC}) has been calculated with all the vibron contributions. The numerical uncertainty is indicated by the thin black error bars. (c) Concentration dependence of the triplet diffusion length calculated with Dexter (triangles), Förster (squares), and combined (circles) transfer integrals for the four emitter molecules in CBP. The average guest-guest distance is defined as $d_{average} \equiv (c_{emitter} \times n)^{-1/3}$ with n the molecular density of the film.

squared Förster transfer integrals dominate over the Dexter transfer integrals at distances larger than 1.5 nm. The diffusion lengths with combined Dexter and Förster couplings are only slightly longer than the largest of the Dexter-only or Förster-only diffusion lengths. This can be explained by the fact that the Dexter and Förster D-A couplings can both enhance or diminish each other, depending on the relative sign of the transfer integrals.

Figure 5(a) also shows that the Marcus theory approximation to ρ_{FC} underestimates the diffusion length in all the emitter systems. However, the effect is not as large as might be expected from the transfer rates shown in Fig. 4(b), where at $\Delta E = 0$ an order of magnitude difference was found between the transfer rates obtained with the full theory for ρ_{FC} and within the framework of Marcus theory. We ascribe this to the very wide distribution of the transfer integrals [see Figs. 3(a) and 3(b)], in combination with the relatively small probability that (in these 10 mol% films) an exciton diffuses before decaying radiatively. The diffusion process often involves at most a single, already quite improbable, transfer process. The effect of a change of the transfer rate by one order of magnitude is therefore relatively small.

The results for the 100 mol% films are shown in Fig. 5(b). In these neat film systems, the strong short-range Dexter coupling between nearest-neighbor molecules is the dominant process. For nearest-neighbor transfer, the squared Dexter coupling is up to four orders of magnitude larger than the squared Förster coupling. Förster coupling contributes therefore only little to the triplet transfer. As the diffusion length is in this case a result of many transfer steps, the difference between the full theory and Marcus theory is larger than for the 10 mol% films, in particular for $Ir(ppy)_3$ and $Ir(BT)_2(acac)$.

Figure 5(c) shows the emitter concentration dependence of the diffusion length, for Dexter-only, Förster-only, and combined transfer. In the 2–10 mol% range, the Förster contribution is dominant or at least comparable with the Dexter contribution. Above approximately 30 mol%, depending on the system, the Dexter contribution is largest.

B. Diffusion on a simple cubic lattice

In the absence of detailed structural information, the actual thin film morphology is in KMC simulations of OLEDs often replaced by a simple cubic (sc) lattice [69,70]. In such simulations, the ΔE dependence of exciton transfer is usually described by the Miller-Abrahams (MA) theory, which does not require molecule-specific knowledge of the vibron spectra and the exciton-vibron interaction strength. The molecule-specific parameters that lead to the transfer integrals (J_{DA}) and the FC weighted density of vibrational states (ρ_{FC}), discussed in this work, are often unknown. Information about the exciton transfer rate can be obtained from dedicated experiments probing the effect of diffusion on the efficiency loss due to, e.g., quenching at defects or due to TTA. It is therefore of interest to compare the Förster radii that would follow from a KMC analysis of experiments probing triplet diffusion when assuming a sc lattice and thermally activated exciton transfer as described using the MA model, with the values that follow from assuming diffusion in the actual morphology and thermally activated transfer as described using the model presented in this paper.

We consider a sc lattice with a lattice constant of 1 nm, containing 10 mol% of randomly dispersed guest molecules, assuming $\sigma_T = 0.05$ eV. Within the MA model, the transfer rate is given by $k = k_{Förster} \exp[-(\Delta E + |\Delta E|)/(2k_B T)]$, with $k_{Förster} = (1/\tau)(R_F/R)^6$. We note that the diffusion length does not depend on τ. The simulations are carried out for $T = 300$ K. Figure 6 (open circles) gives the dependence of the diffusion length on R_F. The colored squares give for the four emitter molecules the diffusion length and the Förster radii

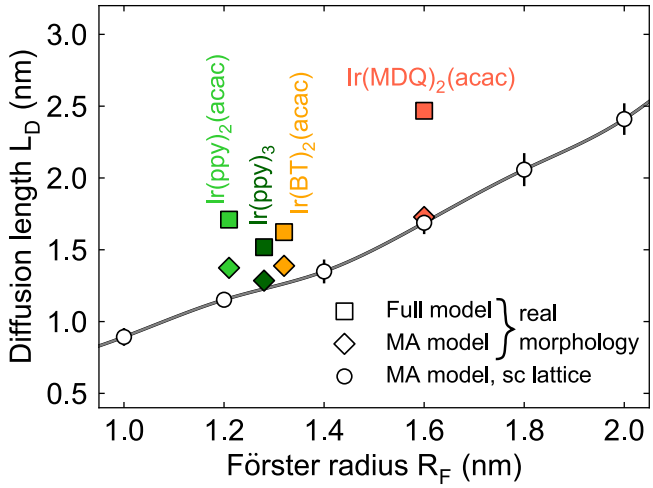

FIG. 6. Results of KMC simulations of the triplet diffusion length for Förster-type emitter-emitter transfer as a function of Förster radius in 10 mol% emitter systems at room temperature. Colored squares: results for realistic morphologies of the four emitters embedded in CBP using the full model for the Förster transfer. The Förster radii on the x-axis are obtained from Table II ($R_{F,0}$). Colored diamonds: the same but with a MA-type vibronic factor $\rho_{MA} = \rho_{FC,eff,0} \exp[-(\Delta E + |\Delta E|)/(2k_BT)]$, with $\rho_{FC,eff,0}$ from Table II. Open circles connected by a curve that serves as a guide to the eye: results for a simple cubic (sc) lattice and triplet energy disorder $\sigma_T = 0.05$ eV using Eq. (12) and the MA model for the energy dependence of the transfer: $k = (1/\tau)(R_F/R)^6 \exp[-(\Delta E + |\Delta E|)/(2k_BT)]$. Unless otherwise indicated, the uncertainties are equal to the symbol size.

calculated at $\Delta E = 0$ (see Sec. III C) for the real morphology and using the full model for the dependence of the transfer rate on ΔE, developed in this paper. For all emitters, the description using a sc lattice and the MA model requires the use of a larger value of R_F than using the realistic morphology and the full model for the rates. The Förster radii that, using the sc lattice and the MA approximation, yield the best fit to the actual diffusion lengths are approximately 1.5 nm for Ir(ppy)$_3$, Ir(ppy)$_2$(acac), and Ir(BT)$_2$(acac), and 2.0 nm for Ir(MDQ)$_2$(acac). The difference is due to neglecting the spatial and orientational disorder and the use of MA theory instead of the FC weighted density of vibrational states. The latter effect is found to have the largest impact. That may be seen from the diamond symbols in Fig. 6, which show simulation results for a real morphology and Förster couplings but with a MA-type vibronic factor ($\rho_{MA} = \rho_{FC,eff,0} \exp[-(\Delta E + |\Delta E|)/(2k_BT)]$). The importance of using the full model for the rates can be understood from Fig. 4(b), which shows that within the full model energetically downward transfer is favored considerably. This effect is not present in the MA rate.

V. SUMMARY AND CONCLUSION

We have developed an *ab initio* model for triplet exciton diffusion due to intermolecular transfer in four phosphorescent emitters that are commonly used in OLEDs: Ir(ppy)$_3$, Ir(ppy)$_2$(acac), Ir(BT)$_2$(acac), and Ir(MDQ)$_2$(acac). Our study includes neat films and 10 mol% films formed by the commonly used host materials CBP and TCTA, containing these emitters as a guest. The triplet transfer rates and the resulting diffusion lengths are expressed as a sum of Förster and Dexter contributions and are calculated for realistic morphologies. The effects of positional, orientational, and energetic disorder are thus included. The molecular reorganization process that occurs upon triplet transfer is described by taking the coupling of triplet states with all intramolecular vibron modes into account, by expressing the rate in terms of the full Franck-Condon weighted density of vibrational states (ρ_{FC}).

Due to the various types of disorder, the Förster and Dexter transfer integrals show both, for a given donor-acceptor distance, a wide distribution. On average, the Förster transfer integrals are larger for an average guest-guest distance above approximately 1.5 nm (20–30 mol%). The Dexter transfer integrals, which are enhanced by at least two orders of magnitude due to coupling via intermediate charge-transfer states, are strongest for average guest-guest distances smaller than 1.5 nm. Each of the four iridium emitters has its own unique vibron spectrum, with associated vibron couplings. These spectra lead in all cases studied to a dependence of the triplet transfer rate on the difference between the final and initial triplet state energies that deviates strongly from the often-used Miller-Abrahams model. Furthermore, for some cases [Ir(ppy)$_3$ and Ir(BT)$_2$(acac)] the transfer rate is enhanced by an order of magnitude or more as compared to the semiclassical Marcus theory.

In the 10 mol% films, the average diffusion lengths are small, close to the average intermolecular distance of around 1.5 nm. Many triplets then do not diffuse before decaying. At this concentration, Förster transfer is the predominant mechanism for all systems studied. In contrast, for 100 mol% emitter films the calculated diffusion length increases to 15–30 nm. Above 30–40 mol% Dexter transfer is the dominant mechanism, and the Förster contribution becomes unimportant. For Ir(ppy)$_3$ and Ir(BT)$_2$(acac), Marcus theory underestimates the diffusion length then by a factor of 2–3.

Finally, we have "translated" the results of our study to KMC simulations assuming a simple cubic lattice and assuming thermally activated exciton transfer as described within the Miller-Abrahams theory, as is commonly done in OLED device simulations. We find that a description of Förster-type diffusion leading to the same diffusion length as obtained from our *ab initio* study would require the use of Förster radii of approximately 1.5 nm for Ir(ppy)$_3$, Ir(ppy)$_2$(acac), and Ir(BT)$_2$(acac), and 2.0 nm for Ir(MDQ)$_2$(acac). These values are 0.2–0.4 nm larger than obtained within our full theory. The difference is mainly due to the use of the Miller-Abrahams rate, which does not account for the favoring of transfers down in energy as in the full theory.

This work unveils the importance of molecule-specific parameters, such as transfer integrals, energetic disorder, and triplet-vibron couplings, in the calculation of triplet diffusion in host-guest systems. Although many different stable and functional iridium-cored phosphorescent emitters have been discovered [71], the molecular parameters determining the transfer rates between these molecules have long remained unknown. The calculational method presented in this work

is expected to support exploring novel routes towards engineering triplet-vibron coupling in order to increase or decrease triplet diffusion.

ACKNOWLEDGMENTS

This research is part of the Horizon-2020 EU projects EXTMOS (Project No. 646176) and MOSTOPHOS (Project No. 646259). This project has received funding from the European Union's Horizon 2020 research and innovation programme under the Marie Skłodowska-Curie Grant agreement MolDesign No. 795206. This work was partially performed on the computational resources ForHLR I and ForHLR II funded by the Ministry of Science, Research and the Arts Baden-Württemberg and DFG ("Deutsche Forschungsgemeinschaft").

[1] C. Adachi, M. A. Baldo, M. E. Thompson, and S. R. Forrest, J. Appl. Phys. **90**, 5048 (2001).
[2] Y. Kawamura, K. Goushi, J. Brooks, J. J. Brown, H. Sasabe, and C. Adachi, Appl. Phys. Lett. **86**, 071104 (2005).
[3] K. H. Kim, S. Lee, C. K. Moon, S. Y. Kim, Y. S. Park, J. H. Lee, J. W. Lee, J. Huh, Y. You, and J. J. Kim, Nat. Commun. **5**, 5769 (2014).
[4] Y. Kawamura, J. Brooks, J. J. Brown, H. Sasabe, and C. Adachi, Phys. Rev. Lett. **96**, 017404 (2006).
[5] R. H. Friend, R. W. Gymer, A. B. Holmes, J. H. Burroughes, R. N. Marks, C. Taliani, D. D. C. Bradley, D. A. Dos Santos, J. L. Brédas, M. Lögdlund, and W. R. Salaneck, Nature (London) **397**, 121 (1999).
[6] J. C. Ribierre, A. Ruseckas, K. Knights, S. V. Staton, N. Cumpstey, P. L. Burn, and I. D. W. Samuel, Phys. Rev. Lett. **100**, 017402 (2008).
[7] M. A. Baldo, C. Adachi, and S. R. Forrest, Phys. Rev. B **62**, 10967 (2000).
[8] W. Staroske, M. Pfeiffer, K. Leo, and M. Hoffmann, Phys. Rev. Lett. **98**, 197402 (2007).
[9] K. S. Son, M. Yahiro, T. Imai, H. Yoshizaki, J. Nishide, H. Sasabe, and C. Adachi, Jpn. J. Appl. Phys. **47**, 7363 (2008).
[10] D. Song, S. Zhao, Y. Luo, and H. Aziz, Appl. Phys. Lett. **97**, 243304 (2010).
[11] Y. Zhang and S. R. Forrest, Chem. Phys. Lett. **590**, 106 (2013).
[12] S. Reineke and M. A. Baldo, Phys. Status Solidi (A) **209**, 2341 (2012).
[13] C. Murawski, K. Leo, and M. C. Gather, Adv. Mater. **25**, 6801 (2013).
[14] N. C. Erickson and R. J. Holmes, Adv. Funct. Mater. **24**, 6074 (2014).
[15] R. Coehoorn, H. Van Eersel, P. A. Bobbert, and R. A. Janssen, Adv. Funct. Mater. **25**, 2024 (2015).
[16] T. Yonehara, K. Goushi, T. Sawabe, I. Takasu, and C. Adachi, Jpn. J. Appl. Phys. **54**, 071601 (2015).
[17] K. W. Hershey and R. J. Holmes, J. Appl. Phys. **120**, 195501 (2016).
[18] L. Zhang, H. van Eersel, P. A. Bobbert, and R. Coehoorn, Chem. Phys. Lett. **662**, 221 (2016).
[19] A. Ligthart, X. de Vries, L. Zhang, M. C. Pols, P. A. Bobbert, H. van Eersel, and R. Coehoorn, Adv. Funct. Mater. **28**, 1804618 (2018).
[20] O. V. Mikhnenko, R. Ruiter, P. W. M. Blom, and M. A. Loi, Phys. Rev. Lett. **108**, 137401 (2012).
[21] X. Liu, Y. Zhang, and S. R. Forrest, Phys. Rev. B **90**, 085201 (2014).
[22] Y. C. Zhou, L. L. Ma, J. Zhou, X. M. Ding, and X. Y. Hou, Phys. Rev. B **75**, 132202 (2007).
[23] B. W. D'Andrade, M. E. Thompson, and S. R. Forrest, Adv. Mater. **14**, 147 (2002).
[24] S. Matthew Menke and R. J. Holmes, J. Mater. Chem. C **4**, 3437 (2016).
[25] D. L. Dexter, J. Chem. Phys. **21**, 836 (1953).
[26] G. D. Scholes and K. P. Ghiggino, J. Chem. Phys. **101**, 1251 (1994).
[27] G. D. Scholes and K. P. Ghiggino, J. Phys. Chem. **98**, 4580 (1994).
[28] R. D. Harcourt, G. D. Scholes, and K. P. Ghiggino, J. Chem. Phys. **101**, 10521 (1994).
[29] G. D. Scholes, R. D. Harcourt, and K. P. Ghiggino, J. Chem. Phys. **102**, 9574 (1995).
[30] R. A. Marcus, J. Chem. Phys. **24**, 966 (1956).
[31] J. Ulstrup and J. Jortner, J. Chem. Phys. **63**, 4358 (1975).
[32] M. Bixon and J. Jortner, Chem. Phys. **176**, 467 (1993).
[33] A. Miller and E. Abrahams, Phys. Rev. **120**, 745 (1960).
[34] T. S. Ahn, N. Wright, and C. J. Bardeen, Chem. Phys. Lett. **446**, 43 (2007).
[35] S. Athanasopoulos, E. V. Emelianova, A. B. Walker, and D. Beljonne, Phys. Rev. B **80**, 195209 (2009).
[36] S. T. Hoffmann, S. Athanasopoulos, D. Beljonne, H. Bässler, and A. Köhler, J. Phys. Chem. C **116**, 16371 (2012).
[37] T. Förster, Ann. Phys. **437**, 55 (1948).
[38] G. D. Scholes, Annu. Rev. Phys. Chem. **54**, 57 (2003).
[39] P. O. Löwdin, J. Chem. Phys. **18**, 365 (1950).
[40] R. Hamze, R. Jazzar, M. Soleilhavoup, P. I. Djurovich, G. Bertrand, and M. E. Thompson, Chem. Commun. **53**, 9008 (2017).
[41] J. Wehner and B. Baumeier, J. Chem. Theory Comput. **13**, 1584 (2017).
[42] P. Siders and R. Marcus, J. Am. Chem. Soc. **103**, 741 (1981).
[43] S. Chaudhuri, S. Hedström, D. D. Méndez-Hernández, H. P. Hendrickson, K. A. Jung, J. Ho, and V. S. Batista, J. Chem. Theory Comput. **13**, 6000 (2017).
[44] M. Etinski, J. Tatchen, and C. M. Marian, Phys. Chem. Chem. Phys. **16**, 4740 (2014).
[45] X. de Vries, P. Friederich, W. Wenzel, R. Coehoorn, and P. A. Bobbert, Phys. Rev. B **97**, 075203 (2018).
[46] E. Buhks, M. Bixon, J. Jortner, and G. Navon, J. Phys. Chem. **85**, 3759 (1981).
[47] A. D. Becke, J. Chem. Phys. **98**, 1372 (1993).
[48] A. Schäfer, H. Horn, and R. Ahlrichs, J. Chem. Phys. **97**, 2571 (1992).
[49] F. Neese, Wiley Interdiscip. Rev. Comput. Mol. Sci. **8**, 4 (2018).

[50] K. Mori, T. P. Goumans, E. Van Lenthe, and F. Wang, Phys. Chem. Chem. Phys. **16**, 14523 (2014).
[51] D. Escudero, Chem. Sci. **7**, 1262 (2016).
[52] C. Brückner and B. Engels, J. Comput. Chem. **37**, 1335 (2016).
[53] T. Neumann, D. Danilov, C. Lennartz, and W. Wenzel, J. Comput. Chem. **34**, 2716 (2013).
[54] See Supplemental Material at http://link.aps.org/supplemental/10.1103/PhysRevB.99.205201 for details on the generation of the morphologies, calculation of the triplet energetic disorder, additional results for the Dexter transfer integrals in the CBP and TCTA hosts, plots of the triplet wave function orbitals, transfer rates calculated at 150 K, and triplet diffusion lengths in a TCTA host.
[55] P. Friederich, F. Symalla, V. Meded, T. Neumann, and W. Wenzel, J. Chem. Theory Comput. **10**, 3720 (2014).
[56] R. Ahlrichs, M. Bär, M. Häser, H. Horn, and C. Kölmel, Chem. Phys. Lett. **162**, 165 (1989).
[57] F. Neese, J. Chem. Phys. **122**, 034107 (2005).
[58] D. A. Pantazis, X.-Y. Chen, C. R. Landis, and F. Neese, J. Chem. Theory Comput. **4**, 908 (2008).
[59] J. Pascual-Ahuir, E. Silla, and I. Tunon, J. Comput. Chem. **15**, 1127 (1994).
[60] Z. T. Liu, C. Y. Kwong, C. H. Cheung, A. B. Djurišić, Y. Chan, and P. C. Chui, Synth. Met. **150**, 159 (2005).
[61] A. Salehi, Y. Chen, X. Fu, C. Peng, and F. So, ACS Appl. Mater. Interfaces **10**, 9595 (2018).
[62] K. Nozaki, J. Chin. Chem. Soc. **53**, 101 (2006).
[63] S. J. Strickler and R. A. Berg, J. Chem. Phys. **37**, 814 (1962).
[64] S. Y. Kim, W. I. Jeong, C. Mayr, Y. S. Park, K. H. Kim, J. H. Lee, C. K. Moon, W. Brütting, and J. J. Kim, Adv. Funct. Mater. **23**, 3896 (2013).
[65] C. Fan and C. Yang, Chem. Soc. Rev. **43**, 6439 (2014).
[66] R. Coehoorn, P. A. Bobbert, and H. van Eersel, Phys. Rev. B **99**, 024201 (2019).
[67] B. C. Lin, C. P. Cheng, and Z. P. M. Lao, J. Phys. Chem. A **107**, 5241 (2003).
[68] P. Friederich, V. Meded, A. Poschlad, T. Neumann, V. Rodin, V. Stehr, F. Symalla, D. Danilov, G. Lüdemann, R. F. Fink, I. Kondov, F. von Wrochem, and W. Wenzel, Adv. Funct. Mater. **26**, 5757 (2016).
[69] M. Mesta, M. Carvelli, R. J. de Vries, H. van Eersel, J. J. M. van der Holst, M. Schober, M. Furno, B. Lüssem, K. Leo, P. Loebl, R. Coehoorn, and P. A. Bobbert, Nat. Mater. **12**, 652 (2013).
[70] H. Van Eersel, P. A. Bobbert, R. A. Janssen, and R. Coehoorn, Appl. Phys. Lett. **105**, 143303 (2014).
[71] M. Thompson, MRS Bull. **32**, 2011 (2011).